

pubs.acs.org/Macromolecules Article

Glassy Dynamics of Epoxy-Amine Thermosets Containing Dynamic, Aromatic Disulfides

Broderick Lewis, Joseph M. Dennis, Cheol Park, and Kenneth R. Shull*



Cite This: Macromolecules 2024, 57, 7112–7122



Read Online

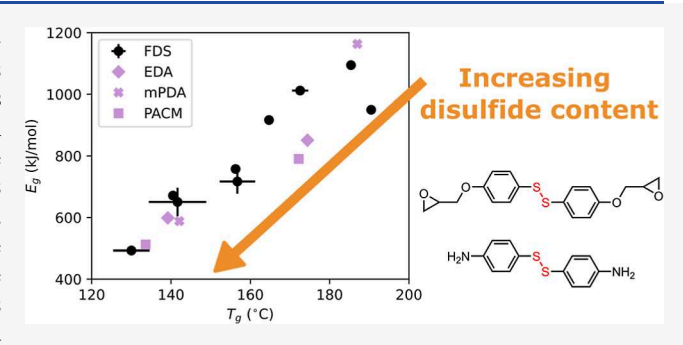
ACCESS

III Metrics & More

Article Recommendations

s Supporting Information

ABSTRACT: Continued progress in understanding the relaxations and mechanical performance of covalent adaptable networks (CANs) will lead to the further adoption of these unique materials across a wide range of applications. Using a model CAN system consisting of dynamic, aromatic disulfides in epoxy-amine thermosets, several network characteristics were found to vary as a function of disulfide concentration and topological placement. The mass density was found to increase significantly with the disulfide concentration, while the glass transition temperature decreased linearly with disulfide content (from 190 to 130 °C), as measured by modulated differential scanning calorimetry and



dynamic mechanical analysis. Furthermore, the apparent activation energy of the glass transition, E_g , as estimated by time—temperature superposition, decreased with increasing disulfide concentration. Significant changes in the sub- T_g relaxations were also observed and correlate strongly with the concentration and placement of disulfide bonds within the network.

■ INTRODUCTION

Thermoset polymers containing dynamic bonds continue to expand in complexity as new chemistries are developed, and the dynamic behavior is characterized. The combination of sufficient exchangeable moieties within a thermoset and a stimulus (e.g., heat or light) allows for topological rearrangement of the network and permits reprocessing of a nominally intractable material. By combining the desirable aspects of thermoset polymers (e.g., mechanical robustness, insolubility, and thermal stability) with the reprocessability of thermoplastic polymers, materials can be developed that possess both high-performance properties and improved sustainability. These dynamic moieties can range in strength from noncovalent interactions such as metal-ligand coordination, 1,2 host-guest complexes, 3,4 and hydrogen bonding 5,6 to dynamic covalent bonds such as (retro-)Diels-Alder reactions,^{7,8} transesterification, 9,10 boronic ester exchange, 11,12 urethane exchange, 13,14 and disulfide exchange, 15-18 with more chemistries being continually adapted for polymeric materials. Polymeric materials that include dynamic covalent bonds are often referred to as dynamic covalent polymers, vitrimers, or covalent adaptable networks (CANs), the latter of which will be used throughout this work. CANs are also divided between associative and dissociative, depending on the exchange mechanism of the dynamic bond present. 19,20 While the detailed assessment of dynamic covalent bonds and their interplay with network dynamics has begun to be established in rubbery, low $T_{\rm g}$ systems, 11,13,19,21 studies of high $T_{\rm g}$ materials is relatively unexplored, perhaps arising from slower molecular diffusion and confounding local relaxations.

For structural applications, engineering polymers require a $T_{\rm g}$ much greater than the intended service temperatures to maintain the desired glassy properties and avoid dramatic softening of the material and ultimately failure of the structural component. It is also preferred to minimize the creep compliance of a material when engineering for structural applications, and highly cross-linked polymer networks usually meet this requirement due to the topological constraints of dense covalent cross-linking; however, the introduction of exchangeable bonds in CANs could dramatically change that behavior, especially at temperatures approaching $T_{\rm g}$. In contrast, accelerating the relaxation kinetics above $T_{\rm g}$ in CANs could facilitate the reprocessing or thermoforming of CAN composites. This dual optimization of creep resistance and facile reprocessing relies heavily on how kinetics change near the glass transition; thus, it is critical to determine how the inclusion of dynamic bonds affects local network dynamics across a broad temperature range. Detailed measurements of relaxation kinetics near $T_{\rm g}$ and above are also useful for the general study of how segmental and dynamic exchange kinetics couple in CANs and other dynamic polymer networks.

Received: May 3, 2024 Revised: June 19, 2024 Accepted: July 10, 2024 Published: July 30, 2024





Table 1. Relative Concentration of Monomers Used for Each Composition in the FDS and Resultant Mole Fraction of Disulfide Bonds in the Networks

FDS compositional table					
name	mol % DGEBA	mol % BGPDS	mol % MDA	mol % DTDA	mol fraction of S-S
DGEBA-MDA	100	0	100	0	0
DGEBA-DTDA50	100	0	50	50	$\frac{1}{6}$
DGEBA-DTDA	100	0	0	100	$\frac{1}{3}$
BGPDS50-MDA	50	50	100	0	$\frac{1}{3}$
BGPDS50-DTDA50	50	50	50	50	$\frac{1}{2}$
BGPDS-MDA	0	100	100	0	$\frac{2}{3}$
BGPDS50-DTDA	50	50	0	100	$\frac{2}{3}$
BGPDS-DTDA50	0	100	50	50	<u>5</u>
BGPDS-DTDA	0	100	0	100	1

Because these dynamic covalent moieties are bound within a network, their ability to exchange will naturally be influenced by the mobility of the network in which they reside. 22-24 The segmental dynamics of polymer networks can vary widely across temperatures, and the most prominent thermal characteristic of a cross-linked network tends to be its glass transition, where the characteristic time scales of segmental dynamics change by many orders of magnitude over a relatively narrow temperature range. In addition to T_{g} , another important concept within glass formation is the apparent or effective activation energy of the glass transition, E_g , which describes the temperature sensitivity of dynamic properties near T_g , as defined by eqs 1 and 2, where x is a dynamic variable (e.g., relaxation time, τ , or viscosity, η), R is the universal gas constant (8.3145 J/mol K), and T is temperature. 25,26 This effective activation energy is similar to the dynamic fragility index, m, (which can be thought of as an effective activation energy normalized by T_g , as given by eq 3), and materials with low E_g are considered strong glass formers and often follow Arrhenius temperature dependences, while those with high $E_{\rm g}$ are considered fragile glass formers and often follow super-Arrhenius temperature dependences. 26,27 The apparent activation energies of many glass-forming materials have been tabulated by Qin and McKenna, 26 and these data illustrate how the $E_{\rm g}$ values observed in most polymeric materials are dramatically greater in magnitude (ca. 200 to 1200 kJ/mol) than many dynamic exchange chemistries used in CANs (ca. 10 to 200 kJ/mol).^{2,10-12,18,28-31} It is important to emphasize that these E_g values are effective or apparent activation energies because they are temperature sensitivities calculated in the same way as usual activation energies, but the glass transition is not simply a thermally activated Arrhenius process; however, the use of E_{σ} provides an intuitive framework for comparing temperature sensitivities among materials.

$$E_{\text{eff}} \equiv R \frac{\partial (\ln x)}{\partial \left(\frac{1}{T}\right)} \tag{1}$$

$$E_{\rm g} \equiv E_{\rm eff}|_{T=T_{\rm g}} \tag{2}$$

$$E_{\rm g} = \ln 10 \, RT_{\rm g} m \tag{3}$$

While relaxation behavior at temperatures near and greater than $T_{\rm g}$ can help determine viable service temperatures and reprocessing conditions, relaxation behavior in the glassy state can also have dramatic implications for properties like toughness in structural materials. These sub- $T_{\rm g}$ relaxations have been analyzed in myriad glass-forming systems and typically correspond with processes like intramolecular motions (e.g., backbone crankshaft fluctuations or aromatic ring flipping) or local cage-like rattling. Because each of these sub- $T_{\rm g}$ relaxations corresponds with local mobility, they can indicate processes that dissipate energy in the material and have been correlated with high toughness.

This work aims to assess how the inclusion of dynamic aromatic disulfide bonds (as a function of both the relative concentration and topological placement within the network) within high- $T_{\rm g}$ epoxy-amine thermosets affects the glassy dynamics of the polymer networks. It is hoped that this study of a model CAN system will help expand the utility of high- $T_{\rm g}$, dynamic glasses by correlating critical relaxation processes and network design to macroscale performance, such as strength and toughness.

MATERIALS AND METHODS

Materials. Diglycidyl ether of bisphenol A (DGEBA), 4,4′-ethylenedianiline (EDA), m-phenylenediamine (mPDA), (±)-epichlorohydrin (ECH), benzyltriethylammonium chloride (BTEAC), potassium iodide (KI), potassium carbonate (K₂CO₃), magnesium sulfate (MgSO₄), and dichloromethane (DCM) were purchased from Sigma-Aldrich and used as received. 4,4′-Methylenebis-(cyclohexylamine) (PACM) was purchased from Sigma-Aldrich and was melted at 80 °C and filtered before use. Bis(4-hydroxyphenyl) disulfide (BHPDS) was purchased from Ambeed and used as received. 4,4′-Dithiodianiline (DTDA) was purchased from Oakwood Chemical and used as received. Isopropyl alcohol was purchased from Fisher Scientific and used as received. 4,4′-Diaminodiphenylmethane (MDA) was purchased from Alfa Aesar and used as received. Methanol was purchased from VWR International and used as received.

Synthesis of Bis(4-glycidyloxyphenyl) Disulfide. Bis(4-glycidyloxyphenyl) disulfide (BGPDS) was synthesized using a

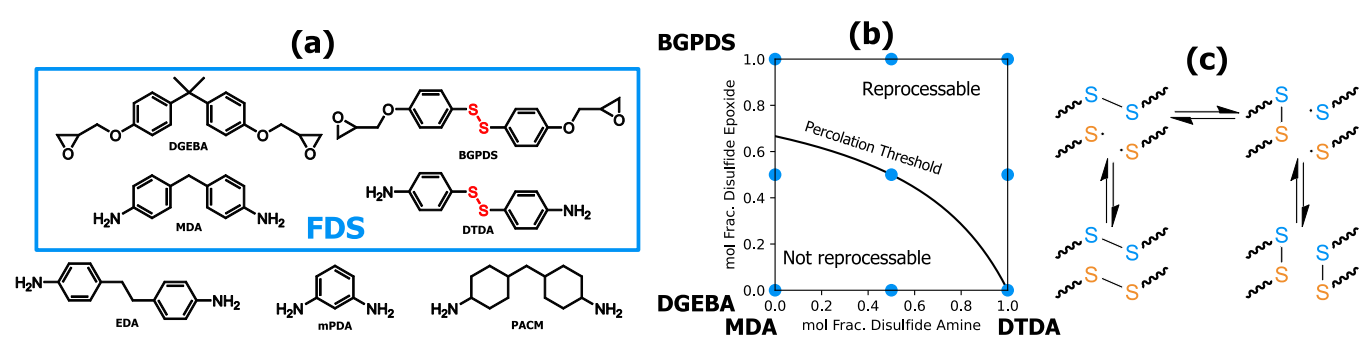


Figure 1. (a) Chemical structures of epoxy and amine components used in this work, where the primary FDS compositions are shown in the blue box and the additional control cross-linkers are shown below. (b) 2D compositional space available when varying content of both dynamic epoxide and amine, with the 9 FDS compositions shown as blue points. (c) Scheme of the radical-mediated disulfide exchange which occurs in the compositions studied.

procedure adapted from those of Takahashi et al. and Memon and Wei.^{39,40} Briefly, 50 g BHPDS, 400 mg KI, and 280 mg BTEAC were dissolved in 400 mL ECH and 80 mL methanol in a 3-neck roundbottom flask and heated to 60 °C under N2 atmosphere and stirred. Then a 50 wt % aqueous solution of K₂CO₃ (48 g of K₂CO₃ in 48 g of DI water) was added to the flask dropwise and allowed to react for 5 h. The reaction mixture was then allowed to cool under stirring, water was added to separate the organic layer, and the organic layer was then washed twice more with DI water. The organic solution was dried over MgSO4, and the excess ECH was distilled off to obtain a crude BGPDS product. To this crude product were then added 400 mg of KI, 280 mg of BTEAC, and 40 mL of methanol, and the mixture was heated to 60 °C under a N2 atmosphere and stirred. Another 50 wt % aqueous solution of K₂CO₃ (48 g K₂CO₃ in 48 g DI water) was added to the flask dropwise and allowed to react for 2 h. The reaction mixture was then allowed to cool under stirring; water and DCM were added to separate the organic layer, and the organic layer was then washed twice more with DI water and dried over MgSO₄. The organic solution was concentrated by distilling off DCM, and the concentrate was then reprecipitated from isopropyl alcohol and dried in a vacuum oven at 60 °C, yielding pure BGPDS (typical yields ∼60-75%). Epoxide equivalent weight (EEW) measurements were made using titrations according to ASTM D1652, and BGPDS batches yielded average EEWs of 190-200 g/eq. ¹H and ¹³C NMR spectra are shown in Figures S1 and S2, respectively.

Preparation of Epoxy Samples. The stoichiometric ratio of epoxide/primary amine was maintained at 2:1 for all formulations. All epoxy compositions were prepared by melting the epoxide and amine components separately, mixing the components vigorously until achieving a homogeneous resin, and degassing the resin at 90 °C in a vacuum oven. The degassed resin was then poured into a rectangular silicone mold (25 mm × 75 mm × 2 mm) and repeatedly degassed and purged with vacuum and N2. All compositions were then precured at 110 °C for 30 min. Compositions were then cured at 160 °C for 8 h or, if their final glass transition temperatures were greater than 160 °C, as measured by differential scanning calorimetry (DSC), they were cured at 160 °C for 2 h and 190 °C for 2 h. These different post-cure schedules are explained further in the Supporting Information (Figure S3). Samples were allowed to cool naturally to room temperature and then were sectioned and polished to dimensions required for additional testing. Table 1 lists the primary compositional series studied, denoted hereafter as the fully dynamic series (FDS). Additionally, six control compositions were created by curing either DGEBA or BGPDS with EDA, mPDA, or PACM. For these control cross-linkers, the relevant mole fraction of disulfide bonds in the network is 0 or $\frac{2}{3}$ when cured with DGEBA or BGPDS, respectively.

Dynamic Mechanical Analysis. Cured resins were sectioned and polished to samples with nominal dimensions of $3 \text{ mm} \times 1 \text{ mm} \times 40 \text{ mm}$. Dynamic mechanical testing was performed on a TA Instruments RSA G2 instrument in tensile geometry with a gap of 30 mm.

Temperature sweeps were performed at 1 Hz with mean tensile strain of 0.1% from -120 to 225 °C at 2.5 °C steps with a 60 s soak at each step. Temperature and frequency sweeps were performed for each composition at $\sim\!T_{\rm g}\pm15$ °C at 2.5 °C steps at frequencies from 0.01 to 10 Hz with mean tensile strain of 0.1%. These dynamic mechanical measurements were performed on all compositions shown as blue points in Figure 1b and the control compositions, and a replicate was tested for the 4 corners and the center point.

Modulated DSC. Temperature-modulated DSC (mDSC) was performed on a TA Instruments DSC250 in TA Zero aluminum pans under a $\rm N_2$ flow. Sample sizes were typically 11–16 mg. In order to erase thermal history, samples were heated to about 50 °C above $T_{\rm g}$ and then cooled to about 50 °C below $T_{\rm g}$ at 3 °C/min with a modulation amplitude of 1 °C and a period of 60 s. All compositions were tested via mDSC in triplicate.

Mass Density Measurements. The mass density of each composition was measured in triplicate using a 20 mL glass pycnometer with water at ambient temperature $(23 \pm 1 \, ^{\circ}\text{C})$.

■ RESULTS AND DISCUSSION

The nine compositions selected for the FDS compositional series (the blue points in Figure 1b) were chosen as a way to probe the extremes of the compositional space along with varying combinations of components to help elucidate the effects of each monomer. This selection also provides several compositions in the nonreprocessable and reprocessable regions, as well as a few near (or on) the mean-field percolation threshold. As defined here, the percolation threshold is meant to signify the boundary between compositions below which, if every disulfide bond were hypothetically broken, there would remain a permanent polymer network of infinite molecular weight. This percolation concept and its implications on reprocessability in CANs have been discussed for a thiol-epoxy system with exchangeable ester moieties by Li et al. The six additional control compositions were studied to assess how well observed trends continue to hold when disulfide bonds are only placed in the diepoxide monomer and the amine cross-linker structure is changed. EDA was used because of the additional carbon atom in the bridge between aromatic carbon rings relative to MDA, mPDA was chosen because the amines are located on a single aromatic carbon ring with no bridge, and PACM was chosen because its structure is similar to that of MDA but with aliphatic carbon rings instead of aromatic ones.

As a way of condensing the 2D compositional space available due to the ability to place disulfide bonds either within the diepoxide or the diamine cross-linker, trends in properties have been plotted against the total mole fraction of

disulfides in the networks to make the visual representations of data simpler. Because of the 2:1 stoichiometric ratio of diepoxide/diamine, increasing the relative concentration of disulfide-containing diepoxide (BGPDS) has a greater increase on the total mole fraction of disulfides than increasing the relative concentration of disulfide-containing diamine (DTDA).

Mass Density. The mass density of each composition was measured because it is an important quantity when designing materials for applications where lightweightness is a key factor and also because it can provide an indication of the relative packing density of the polymer network. As shown in Figure 2,

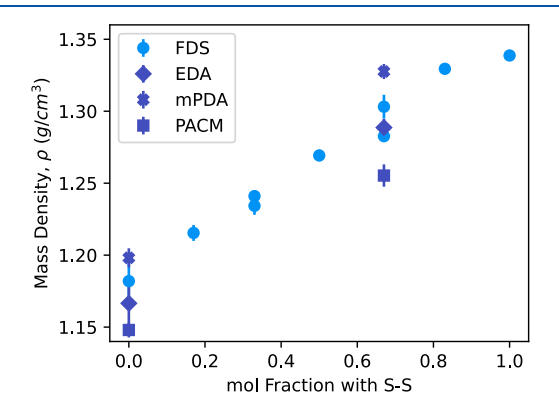


Figure 2. Trends in bulk mass density for each composition studied.

as the relative concentration of disulfide bonds within the network increases, the bulk mass density of the composition increases almost linearly. This trend holds across the FDS compositional series and the control cross-linker compositions. While most of the increase in density that occurs when including disulfide-containing monomers could be due to the heavier atomic mass of sulfur (see Figure S4), some could also be due to more efficient packing of network segments allowed by the more flexible disulfide bonds. It has been reported that more flexible segments tend to allow increased packing density, 42,43 and DFT simulations of these and similar aromatic disulfide-containing monomers have reported a "folded" conformation around the disulfide bond, which could allow improved packing relative to a more rigid, linear segment.³¹ Changes in effective packing fraction (even of only a few percent) can have dramatic impacts on the behavior of materials in the glassy state, 43,44 and the implications of the changes in bulk density observed here will be discussed along with the relevant properties throughout this work.

It is worth noting that for the points where two compositions have an equal mole fraction of disulfides in the network (i.e., at $\frac{1}{3}$ and $\frac{2}{3}$), the composition with more BGPDS present always has the slightly higher density. This would suggest that, although the disulfide bonds are present in the same molar concentration relative to the overall network, BGPDS allows slightly more effective packing than DTDA. This relatively increased packing effectiveness could be because the disulfide bond present in BGPDS is less topologically restricted than in DTDA (i.e., the aromatic disulfide moiety in DTDA is "tethered" at four points due to the diamine's tetrafunctionality, while the aromatic disulfide moiety in BGPDS is "tethered" only at two points due to the diepoxide's bifunctionality) or it could also be due to the additional flexibility of the ether linkages present in BGPDS between the

aromatic disulfides and the cross-linking sites. When BGPDS replaces DGEBA, the absence of the methyl groups in the isopropylidene bridge in DGEBA could also reduce the local free volume, causing an increase in mass density.⁴⁵

The general trend of density among the control cross-linker compositions [i.e., $\rho(\text{mPDA}) > \rho(\text{MDA}) > \rho(\text{EDA}) >$ $\rho(PACM)$ is likely due to differences in local free volume or relative cohesive energy density of the amine cross-linkers. Specifically, as the cross-linker monomers become longer, there will tend to be increased free volume in the network, resulting in reduced mass density, and aliphatic carbon rings in place of aromatic ones (in the case of PACM) would also result in increased free volume and thus lower mass density. Positron annihilation lifetime spectroscopy is a technique that could potentially probe the length scales necessary to determine if the relative free volume in these materials also decreases with increasing disulfide concentration, which would provide further evidence of more efficient packing of the network in the glassy state, 46,47 and the authors intend to use this method in the future to continue investigating the local glassy dynamics of this model system.

Modulated DSC. mDSC experiments were performed on each composition as a method to assess how the inclusion of disulfide linkages within the epoxy-amine networks influences the glass transition characteristics. The characteristics most easily accessible via mDSC are properties such as the glass transition temperature, $T_{\rm g}$, transition breadth, δT , and transition specific heat capacity step change, Δc_p (see Figure S5). By using mDSC, it is simpler to deconvolute reversible and nonreversible/kinetic heat flow components, allowing direct calculation of the reversing specific heat capacity, c_p , and its derivative with respect to temperature through the glass transition. 48,49

Glass transition temperatures, T_g , were determined as the inflection point of c_p in the transition region, or equivalently as the maximum in $\mathrm{d}c_p/\mathrm{d}T$, and are shown as a function of disulfide inclusion in Figure 3. There appears to be a clear,

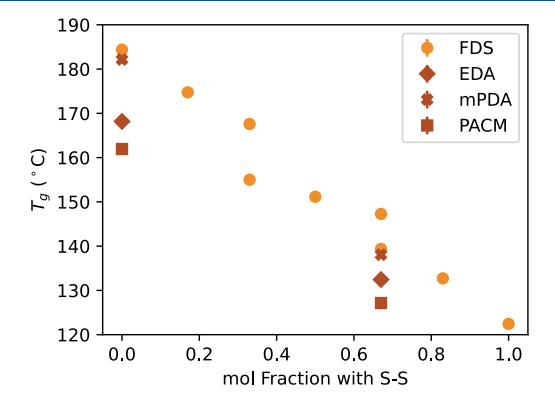


Figure 3. Trends of glass transition temperature, T_g as measured by mDSC for each composition studied.

relatively linear decrease in $T_{\rm g}$ with increasing inclusion of disulfide bonds within the network, which could be expected because when disulfides are included in the networks, they are replacing a significantly stiffer methylene or isopropylidene bridge when included through the diamine or diepoxide, respectively. As the network becomes more flexible on average, it is expected that material $T_{\rm g}$ would decrease. It is again worth noting that for the points where two compositions have an equal mole fraction of disulfide bonds in the network

(i.e., at $\frac{1}{3}$ and $\frac{2}{3}$), the composition with more BGPDS present always has the lower $T_{\rm g}$ [as also observed via dynamic mechanical analysis (DMA) below. This more dramatic lowering of the glass transition temperature would suggest that disulfide bonds included via BGPDS are more flexible than those included via DTDA, due to either the topological "tethering" logic mentioned above in relation to the density differences and/or the additional ether linkages present in the BGPDS structure. Among the control cross-linkers, while the use of mPDA in place of MDA seems to cause little change in Tg, the use of EDA and PACM both seem to cause a lowering of the glass transition temperature relative to MDA, with PACM exhibiting the lowest $T_{\rm g}$ s of the nondynamic crosslinkers tested. These decreased glass transition temperatures could again be expected, as the ethylene bridge between the aromatic carbon rings present in EDA is more flexible than the methylene bridge present in MDA, and the aliphatic carbon rings in PACM are much more flexible than the aromatic carbon rings in MDA.

Temperature Sweeps and Time-Temperature Superposition. Temperature sweeps were performed on each composition as a method to determine the viscoelastic properties over a broad range of temperatures, which is useful for determining potential application temperatures and for identifying features like sub- $T_{\rm g}$ relaxations and the glass transition. Although there is no universally accepted nomenclature for these relaxations, one common practice is to assign each relaxation a Greek letter in descending temperature order (starting with the glass transition as the α relaxation, then the next highest temperature as the β relaxation, and so on). 25,35,51 Example temperature sweeps are shown for the completely nondynamic composition DGEBA-MDA (Figure 4a) and completely dynamic composition BGPDS-DTDA (Figure 4b) with a few points of interest noted (see Figures S6-S23 for all temperature sweeps). At the higher temperatures, the relatively sharp and intense α relaxation peak, or glass transition peak, is noted, and the temperature at which the maximum in this tan δ peak occurs is denoted as T_g in this work. At lower temperatures, two broader and less intense sub- $T_{\rm g}$ relaxation peaks are labeled. Specifically the one present around -60 °C is labeled as the β peak according to convention, as this relaxation is commonly observed in epoxy-amine materials and is attributed to the motion of the dangling glycerol groups that form at the epoxide-amine cross-linking reaction sites. 35,36 The other sub- $T_{\rm g}$ peak, occurring around 10-50 °C, has been labeled as the β' peak to distinguish it from the more typical β relaxation which occurs in epoxy-amine thermosets. These lower temperature relaxations will be discussed in more detail below.

Figure 4c summarizes the measured $T_{\rm g}$ s for each composition studied, clearly illustrating a relatively linear decrease in $T_{\rm g}$ with an increasing molar fraction of disulfide bonds among all the FDS and control compositions. The observed trends are essentially identical to those regarding $T_{\rm g}$ as measured using mDSC, which are discussed in more detail. It is worth mentioning that the $T_{\rm g}$ s as defined here for DMA are systematically a few degrees higher than those as measured via mDSC. This slight variation in $T_{\rm g}$ as measured with different techniques is common and highlights that the glass transition occurs over a range of temperatures and is highly dependent upon time and length scales of the experiment.²⁵

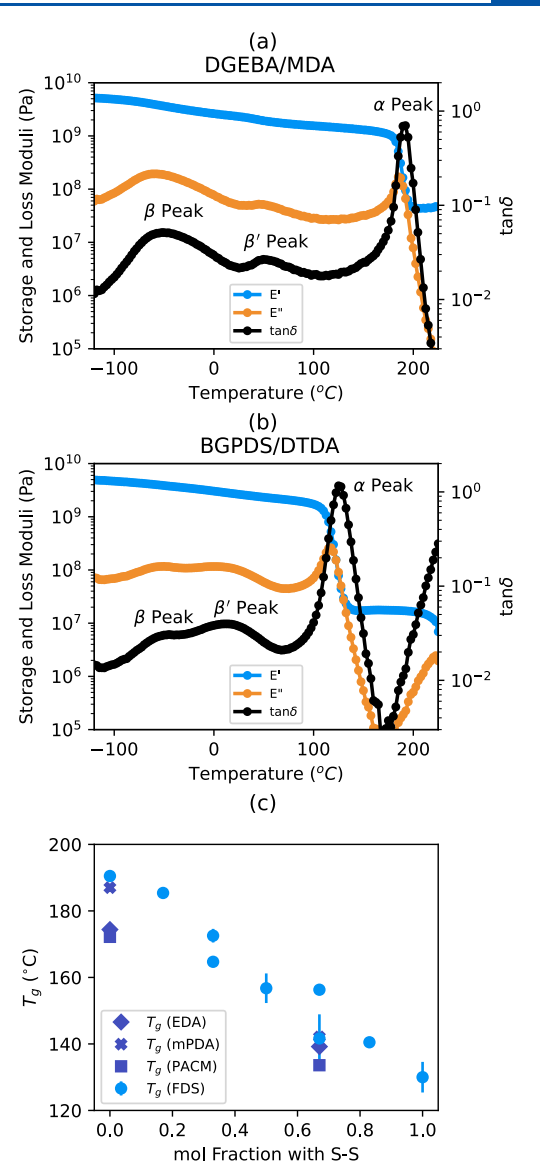


Figure 4. Example temperature sweeps for a completely nondynamic composition (a) and a reprocessable, dynamic composition (b). (c) Trends of glass transition temperature as measured by DMA for all compositions studied.

Another observation worth noting in Figure 4b is the sudden decrease of the storage modulus (and increase in the loss modulus and tan δ) at temperatures exceeding about 200 °C, which also occurs in the other networks containing dynamic disulfide bonds (see Figures S6-S23). This deviation from the rubbery plateau is reminiscent of a terminal flow regime present in thermoplastic polymers and likely corresponds with a dramatic softening of the material due to the relatively facile topological rearrangement afforded by disulfide exchange at these temperatures. This deviation from the rubbery plateau was only observed in compositions containing disulfide bonds, and while the onset of this deviation occurred at similar temperatures in nearly all the systems studied here (likely driven by concerted disulfide exchange relaxation times dropping below about one s), a more rigorous rheological study will be performed on this model system to elucidate the exchange kinetics in more detail and how the disulfide relaxation relates to disulfide concentration and topological placement and is coupled to the segmental dynamics.

To analyze the changes in the segmental dynamics near the glass transition as a function of disulfide inclusion within the networks, temperature and frequency sweeps were completed on each composition near $T_{\rm g}$ so that time—temperature superposition (tTS) could be performed. Horizontal shifting was performed manually with the temperature step nearest the composition $T_{\rm g}$ used as the reference temperature, and an example master curve is shown in Figure 5, illustrating the

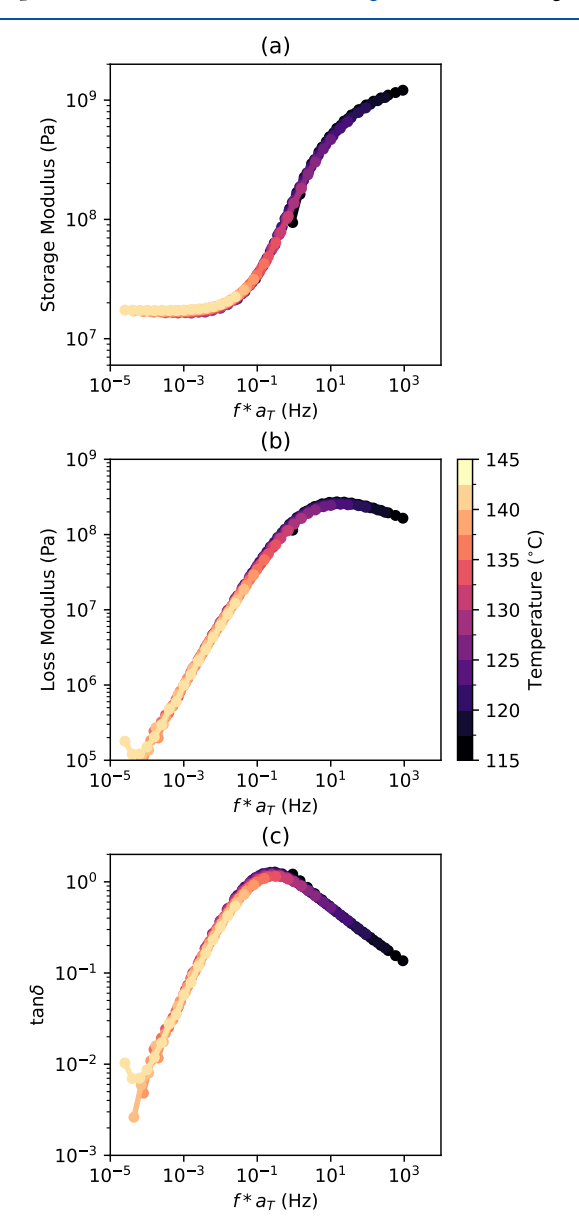


Figure 5. Example tTS master curves for the fully dynamic composition (BGPDS/DTDA) for storage modulus, E', (a); loss modulus, E'', (b); and tan δ (c).

appropriateness of tTS within this temperature range. The unshifted and shifted curves for all compositions are compiled in the Supporting Information (Figures S24–S83). The shift factors (a_T) for each composition were then fit to a Vogel–Fulcher–Tammann (VFT) form (eq 4), where x represents a dynamic variable such as relaxation time (τ) or viscosity (η) , x_0 represents the high temperature limit of that variable, T is absolute temperature, T_0 is a fitting temperature to set the divergence of the property, and B is a material fitting

parameter. An example of this VFT fitting using the shift factors to create the master curves in Figure 5 is shown in Figure 6a, and the fits for all compositions are given in the

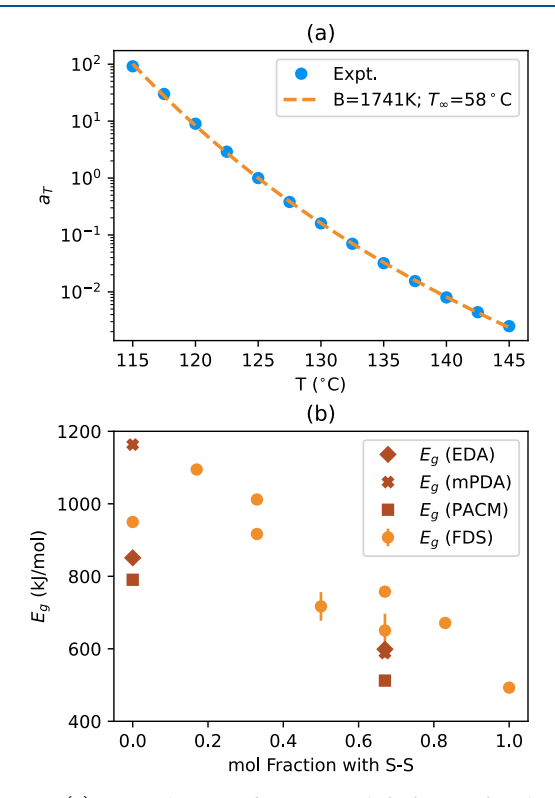


Figure 6. (a) Example VFT fit to tTS shift factors for the fully dynamic composition (BGPDS/DTDA). (b) Trends of apparent activation energy, $E_{\rm gr}$ for all compositions studied.

Supporting Information (see Figures S24–S83). The VFT form is often employed for certain relaxations, like the glass transition, because it captures the super-Arrhenius temperature dependence which occurs. ^{25,26,52} It is also worth noting that the VFT equation is equivalent to the commonly used Williams–Landel–Ferry form.

$$x(T) = x_0 \exp\left(\frac{B}{T - T_0}\right) \tag{4}$$

$$E_{g,VFT} = \frac{RB}{\left(1 - \frac{T_0}{T_g}\right)^2} \tag{5}$$

By fitting the tTS shift factors for each composition to the VFT model, the effective activation energy at the glass transition, $E_{\rm g}$, could be analytically calculated according to eq 5. The calculated $E_{\rm g}$ values for each composition are shown in Figure 6b. As can be seen, there appears to be a general trend of decreasing $E_{\rm g}$ as the relative concentration of disulfide bonds within the network increases. This overall decrease in effective activation energy with disulfide bond inclusions is likely due to the increase in network flexibility as carbon linkages are replaced with disulfides. This relationship of stronger glass formation (i.e., lower $E_{\rm g}$ or fragility) with more flexible networks has both experimental and simulation support. The relationship between $E_{\rm g}$ and $T_{\rm g}$ is also shown in Figure 7, where a relatively linear relationship is observed (and this range of $E_{\rm g}$ s and $T_{\rm g}$ s would lie on the right-hand side of the

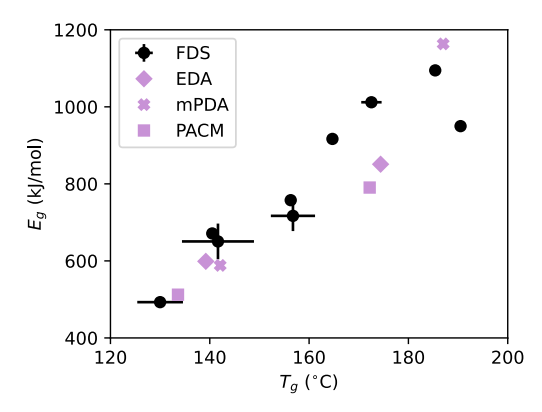


Figure 7. Cross-plot of apparent activation energy at the glass transition, $E_{\rm g}$, and glass transition temperature, $T_{\rm g}$, for all compositions studied.

cloud of polymer glass former data collected in Figure 3 of the work by Qin and McKenna²⁶). This linear relationship makes sense for this material system, where the general cohesive energy density and reactive chemistry are held constant while the average flexibility of the network is systematically increased (by increased inclusion of disulfide linkages). A potential influencing factor of the general trend of decreasing dynamic $E_{\rm g}$ with increasing disulfide inclusion could also be the relative packing density of the network. Again, if the increase in bulk density of the materials with a higher disulfide content is due to an increase in the relative packing density of the glass, this increase in effective packing fraction could also lead to the decrease in effective activation energy. Heterogeneities of packing density within the network caused by differences in the spatial distribution of disulfide bonds (especially in compositions with mixed diepoxide and/or diamine constituents) could alternatively lead to packing frustrations and relatively higher E_g , which could explain why, although there is a general decrease in E_g with disulfide inclusion, this relationship is somewhat "noisy". ^{27,54} The fact that this trend is not as "clean" or idealized as that of the glass transition temperature helps to illustrate the importance of assessing material properties such as effective activation energy near $T_{\rm g}$ when characterizing these types of materials (which are especially relevant when broadly considering the healability and reprocessability kinetics of CANs) because the relationship depends on both chemical and topological parameters. For those points where two compositions have an equivalent mole fraction of disulfide bonds, the composition with greater inclusion of the disulfidecontaining diepoxide BGPDS has the lower E_{σ} , which, again, is likely due to the slightly greater flexibility of BGPDS relative to the disulfide-containing diamine DTDA. When comparing effective activation energies of the glass transition among the control compositions when no disulfide bonds are included in the network, the trend follows the expected relative flexibility of the cross-linkers [i.e., $E_g(mPDA) > E_g(MDA) > E_g(EDA) >$ $E_{g}(PACM)$]; however, the trend is not as consistent when BGPDS is used as the diepoxide, and all the E_{g} s are relatively similar (while the composition with PACM as cross-linker still has the lowest $E_{\rm g}$ among the control cross-linkers). This alteration to the trend in $E_{\rm g}$ would suggest that the increased flexibility due to the presence of disulfides in the epoxide component of the network dominates the decrease in effective activation energy of the glass transition, especially among the aromatic amine cross-linkers.

When comparing the effective activation energies to those of relevant dynamic exchange chemistries, it is important to reiterate how much greater the glass forming temperature sensitivities (i.e., E_e s) are in magnitude. If the segmental dynamics influence the exchange kinetics (and thus the overall measured relaxation kinetics of a network), which is almost certain near T_g and possible even at higher temperatures, then the effective activation energies of glass formation will influence the temperature sensitivities measured through experiment (e.g., stress relaxation).⁵⁵ As an example, if we extend the calculation of the apparent activation energy through the VFT fitting of the BGPDS/DTDA system (which has the lowest E_g values of the FDS compositions studied in this work) to temperatures greater than T_g using eq 1, the effective activation energy, $E_{\rm eff}$, would reach values comparable to the aromatic disulfide bond dissociation energy (e.g., 180 kJ/mol) around 190-195 °C. For more fragile glass-forming materials, this "crossover" temperature would be even higher (see Table S1), suggesting how the temperature sensitivity of the dynamic properties in the temperature range at which these materials would be feasibly reprocessed is almost certainly strongly influenced by the network dynamics. This influence on the temperature sensitivity emphasizes how important it is to account for the glass formation kinetics and segmental dynamics in attempts to accurately measure the exchange kinetics and reprocessability of CANs. The dramatic (super-Arrhenius) reduction in relaxation kinetics due to the sluggish network dynamics also illustrates the inappropriate nature of determining a topological freezing temperature, T_v , by extrapolation if $T_{\rm v}$ is anywhere near the $T_{\rm g}$, as recently discussed by Martins and co-workers.²¹

It is desirable to be able to reprocess and heal CAN materials under the mildest conditions possible because this corresponds with a safer and less energy intensive procedure and also helps to avoid material degradation. Because these materials have relatively high glass transition temperatures among CANs and because the disulfide exchange that allows reprocessing and healing cannot occur appreciably below T_{g} , detailed understanding of the relaxation/exchange kinetics and dynamics near $T_{\rm g}$ (via effective activation energy) can help to find the mildest conditions necessary for stimulating sufficient segmental dynamics to facilitate disulfide exchange and thus heal/reprocess the network. Combining this study with additional dynamics work (e.g., stress relaxation and isothermal creep) at temperatures greater than $T_{g'}$ where the relaxation behavior is likely controlled primarily by the disulfide exchange kinetics, will help to deconvolute segmental and exchange behavior, to gain detailed understanding of the transition between dominant relaxation mechanisms in highly crosslinked networks, and to optimize these and similar CAN materials for both reprocessability and creep resistance via chemical and topological engineering.

Sub- $T_{\rm g}$ **Relaxations.** As mentioned above, two distinguishable sub- $T_{\rm g}$ relaxations were observed in the compositions studied: the typical β relaxation peak ubiquitous in epoxyamine networks, which has been shown to correspond with the activated motion of dangling glycerol groups present at the epoxide-amine cross-linking sites around -60 to -50 °C, 17,35,36 and an additional relaxation observed at temperatures between about 10 and 50 °C, which is denoted β' in this study. To analyze the details of the sub- $T_{\rm g}$ relaxations, the tan δ data for each temperature sweep were baselined between -120 °C and the local minimum just before the onset of the α

relaxation peak. These tan δ data were then fit to two Gaussian peaks so that the relaxation peak temperature, breadth, amplitude, and area could be calculated to compare the relative location and intensity of each sub- $T_{\rm g}$ relaxation across each composition. The peak temperatures for both relaxations for each composition are shown in Figure 8a, and the areas of the relaxations, representative of their relative intensity, for each composition are shown in Figure 8b.

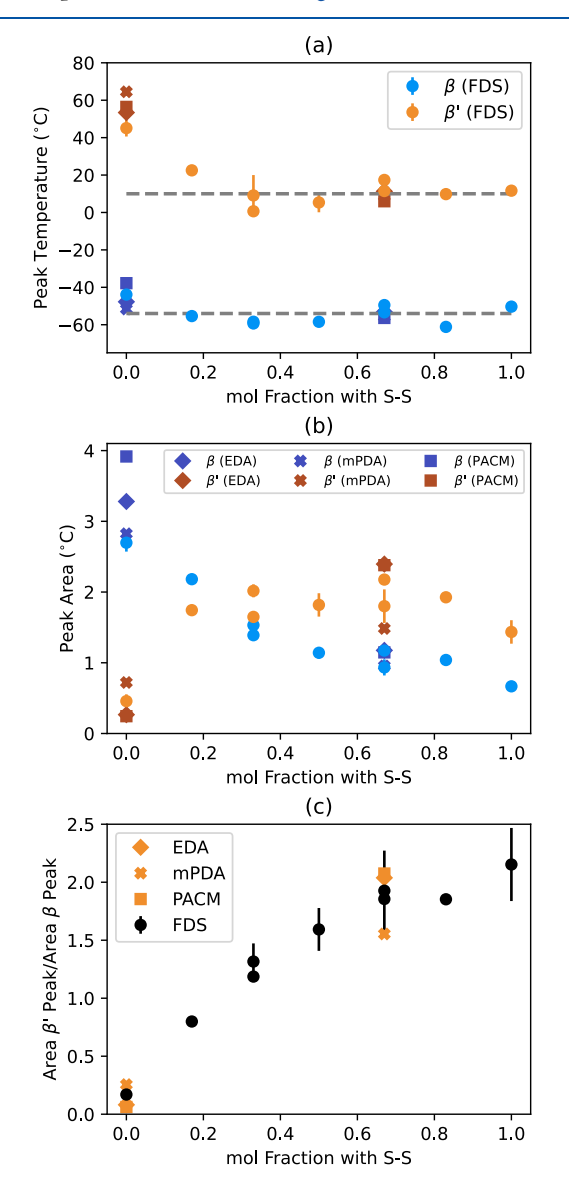


Figure 8. (a) Temperatures corresponding to the center of Gaussian fits to β and β' peaks for each composition. The upper and lower dashed gray lines are guides to the eye at 10 and $-54\,^{\circ}\text{C}$, respectively. (b) Total areas of Gaussian fits to β and β' peaks for each composition. (c) Normalized areas of β'/β peaks for each composition.

The peak temperature at which the β relaxation occurs is essentially constant across all compositions (with an average of -54 °C for the FDS), which could be expected because this relaxation is attributed to the presence of the dangling glycerol groups which form at the epoxide-amine cross-linking reaction sites, 17,35,36 which are present in all systems. Meanwhile, it can be seen that the relative area of the β relaxation decreases with an increasing concentration of disulfide bonds in the network.

This decrease in relative intensity can likely be attributed to the relative decrease in apparent cross-linking density, which occurs as the network becomes more flexible on average with the inclusion of more disulfide bonds (see Figure S87); 35,56,57 however, there is also a relatively insignificant difference in β relaxation intensity between the compositions with equal mole fraction of disulfide bonds, so additional study with techniques like dielectric spectroscopy could help elucidate the details of these changes more precisely. The trend in relative β relaxation intensity among the control compositions without disulfide bonds (i.e., PACM > EDA > mPDA ≈ MDA) could possibly be explained by an increased breadth of the relaxation. In the case of DGEBA-EDA, the additional methylene group between the aromatic rings of the cross-linker provides additional free volume which could allow more secondary relaxation modes or at least a more heterogeneous activation of them. In the case of DGEBA-PACM, both the intensity and breadth of the transition likely increases due to the presence of cycloaliphatic groups (in place of the aromatic rings as in MDA), as observed previously in polyester glasses.³⁴

The behavior of the β' relaxation appears to change dramatically depending on whether disulfide linkages are included in the network. For those compositions without any disulfides, the peak temperature occurs on average at 55 °C, whereas for all compositions with disulfide bonds present (seemingly regardless of relative concentration), the peak temperature occurs on average at 10 °C. The relative area of the β' relaxation also changes dramatically when disulfide bonds are present in the network, with a relatively negligible area/intensity for those compositions without any disulfides and a relatively intense β' peak for those compositions with disulfides. The β' relaxation even becomes more intense than the β relaxation for all compositions containing disulfides, except for the material with the lowest concentration of disulfide bonds (i.e., DGEBA/DTDA50). Figure 8c shows the trend of the β' peak area normalized by the area of the β peak to illustrate the apparent correlation of this additional sub- T_{σ} relaxation with the relative concentration of disulfide linkages in the network. The significant shift in both the temperature at which the relaxation occurs and the relative intensity would suggest that the β' relaxation present in the networks without any disulfide bonds likely has an origin distinct from the β' relaxation occurring in the disulfide-containing compositions. When comparing compositions with an equal mole fraction of disulfide bonds, there is very little difference between their sub- T_g responses when observed in the normalized representation in Figure 8c. This similar response suggests that the topological placement of disulfide bonds within the network (i.e., via the diepoxide or diamine) has a less significant effect than the overall relative concentration of disulfides. The trend in relative β' relaxation intensity among the control compositions with disulfide bonds is somewhat weak, but follows an approximate trend of PACM ≈ EDA > MDA > mPDA, which suggests that the relative flexibility of the cross-linker used can influence the β' relaxation, but that it tends to be a secondary effect, at least among the relatively stiff cross-linkers chosen here.

While the β' relaxation intensity clearly seems to correlate with the presence of disulfide bonds within these network materials (and occurs at a distinct temperature from the significantly less intense β' relaxation existing in the compositions without any disulfide bonds), it is difficult to determine if the relaxation actually corresponds with activated

motion of the disulfide linkages themselves (like how the β relaxation corresponds with the activated motion of dangling – OH groups) or has another molecular origin. It could be that the β' relaxation in all compositions corresponds with a "cagerattling" or Johari-Goldstein-type relaxation, which onsets prior to the glass transition,²⁵ and that the inclusion of disulfide bonds (even at relatively low concentrations) causes a significant change on the activation temperature of this process and its relative intensity. Additional experiments on this model system using techniques like dielectric spectroscopy are needed to more confidently determine the origin of these β' relaxations, which is important not only for fundamental understanding of the glassy physics involved in these and similar dynamic systems but also for optimization of these sub- $T_{\rm g}$ relaxations as a way of tuning mechanical properties and fracture behavior for structural applications of reprocessable thermoset networks.

CONCLUSIONS

This work studied how the inclusion of aromatic disulfide bonds in highly cross-linked epoxy-amine thermosets (as a function of both relative concentration and topological placement) changed various network characteristics within the glass. The bulk mass density was found to increase significantly with increasing mole fraction of disulfide bonds in the network (from 1.18 to 1.34 g/cm³) with the inclusion of disulfides via the diepoxide (i.e., BGPDS in place of DGEBA) having a slightly more significant effect than inclusion via the diamine cross-linker (i.e., DTDA in place of MDA). Although most of this increase in mass density is due to the higher atomic mass of sulfur (as compared to the hydrocarbon linkages, the disulfides are replacing), the more flexible disulfides could also be causing slightly increased effective packing in the networks, which could also explain some of the increase in density and changes observed in other glassy characteristics.

The glass transition temperature was found to decrease relatively linearly (from about 190 to 130 °C) as a function of disulfide concentration within the network, as measured by the inflection point in the step change of heat capacity in mDSC and the peak in tan δ from DMA temperature sweeps; however, for compositions with equivalent overall mole fraction of disulfide bonds in the network, compositions with greater inclusion of disulfides via the diepoxide component had lower $T_{\rm g}s$. This increased depression of $T_{\rm g}$ due to disulfide inclusion in the diepoxide (as compared to inclusion of disulfides in the diamine cross-linker) could be because the diepoxides are effectively bound to the network by two points as opposed to four points in the diamine cross-linkers, so the additional flexibility of the disulfide bond (and thus the overall network) is more pronounced.

By performing both temperature and frequency sweeps for each composition near its respective $T_{\rm g'}$ tTS was performed, and the horizontal shift factors were fit to VFT forms. By performing VFT fits, the effective activation energy of the glass transition, $E_{\rm g'}$ was calculated for each composition, which allowed a comparison of how the relative temperature sensitivity of dynamic variables changes with aromatic disulfide inclusion within the networks. It was found that $E_{\rm g}$ generally decreased with increased mole fraction of disulfide bonds in the network (from over 1000 to about 500 kJ/mol), which can be expected as the network becomes more flexible on average, and, again, it was found that inclusion of disulfides through the

diepoxide had a more pronounced decrease in $E_{\rm g}$ when compared to inclusion through the diamine.

Two distinct sub- $T_{\rm g}$ relaxations were also observed in the DMA temperature sweeps, denoted as the β and β' relaxations. The β relaxation, which is ubiquitous in epoxy-amine materials and typically occurs around $-60~{\rm ^{\circ}C}$, was observed to decrease in relative intensity with increased inclusion of disulfide bonds, likely because of the decrease in apparent cross-link density as the network becomes more flexible on average. The β' relaxation was observed to increase in relative intensity and decrease in peak temperature when disulfides were included within the network but remain relatively constant as a function of mole fraction of disulfide bonds in the network. While the presence of this additional sub- $T_{\rm g}$ relaxation clearly seems to correlate with the presence of aromatic disulfide bonds in the thermosets, additional investigation (e.g., via dielectric spectroscopy) is needed to clarify its molecular origins.

ASSOCIATED CONTENT

Supporting Information

The Supporting Information is available free of charge at https://pubs.acs.org/doi/10.1021/acs.macromol.4c01012.

NMR spectra of dynamic epoxide BGPDS; DSC cure study; density prediction comparison; additional mDSC parameters; additional DMA temperature sweeps; unshifted and shifted tTS data and VFT fits; plots of dynamic fragility against disulfide concentration and cross-plot with $T_{\rm g}$; $E_{\rm eff}$ predictions and comparisons; additional sub- $T_{\rm g}$ relaxation fitting parameters; and apparent cross-link density vs disulfide concentration (PDF)

■ AUTHOR INFORMATION

Corresponding Author

Kenneth R. Shull — Department of Materials Science and Engineering, Northwestern University, Evanston, Illinois 60208, United States; Occid.org/0000-0002-8027-900X; Email: k-shull@northwestern.edu

Authors

Broderick Lewis — Department of Materials Science and Engineering, Northwestern University, Evanston, Illinois 60208, United States; oorcid.org/0009-0009-4607-7939

Joseph M. Dennis – Combat Capabilities and Development Command, Army Research Laboratory, Aberdeen Proving Ground, Maryland 21005, United States; orcid.org/ 0000-0001-9511-4243

Cheol Park – Advanced Materials & Processing Branch, NASA Langley Research Center, Hampton, Virginia 23666, United States

Complete contact information is available at: https://pubs.acs.org/10.1021/acs.macromol.4c01012

Notes

The authors declare no competing financial interest.

ACKNOWLEDGMENTS

The authors would like to thank Dr. Jack F. Douglas for very useful discussions. This work was supported by the NASA Space Technology Graduate Research Opportunity and by the National Science Foundation (NSF) under grants OISE-1743748 and DMR-2308601. This work made use of the

MatCI and CLaMMP Facilities, which receive support from the MRSEC Program (NSF DMR-2308691) of the Materials Research Center at Northwestern University.

REFERENCES

- (1) Mozhdehi, D.; Ayala, S.; Cromwell, O. R.; Guan, Z. Self-Healing Multiphase Polymers via Dynamic Metal—Ligand Interactions. *J. Am. Chem. Soc.* **2014**, *136*, 16128—16131.
- (2) Zhang, X.; Vidavsky, Y.; Aharonovich, S.; Yang, S. J.; Buche, M. R.; Diesendruck, C. E.; Silberstein, M. N. Bridging Experiments and Theory: Isolating the Effects of Metal—Ligand Interactions on Viscoelasticity of Reversible Polymer Networks. *Soft Matter* **2020**, *16*, 8591–8601.
- (3) Nakahata, M.; Takashima, Y.; Yamaguchi, H.; Harada, A. Redox-Responsive Self-Healing Materials Formed from Host-Guest Polymers. *Nat. Commun.* **2011**, *2*, 511.
- (4) Nakahata, M.; Takashima, Y.; Harada, A. Highly Flexible, Tough, and Self-Healing Supramolecular Polymeric Materials Using Host—Guest Interaction. *Macromol. Rapid Commun.* **2016**, *37*, 86–92.
- (5) Yanagisawa, Y.; Nan, Y.; Okuro, K.; Aida, T. Mechanically Robust, Readily Repairable Polymers via Tailored Noncovalent Cross-Linking. *Science* **2018**, *359*, 72–76.
- (6) Zhang, C.; Yang, Z.; Duong, N. T.; Li, X.; Nishiyama, Y.; Wu, Q.; Zhang, R.; Sun, P. Using Dynamic Bonds to Enhance the Mechanical Performance: From Microscopic Molecular Interactions to Macroscopic Properties. *Macromolecules* **2019**, *52*, 5014–5025.
- (7) Kennedy, J. P.; Castner, K. F. Thermally Reversible Polymer Systems by Cyclopentadienylation. II. The Synthesis of Cyclopentadiene-Containing Polymers. J. Polym. Sci. 1979, 17, 2055–2070.
- (8) Terryn, S.; Brancart, J.; Roels, E.; Verhelle, R.; Safaei, A.; Cuvellier, A.; Vanderborght, B.; Van Assche, G. Structure—Property Relationships of Self-Healing Polymer Networks Based on Reversible Diels—Alder Chemistry. *Macromolecules* **2022**, *55*, 5497–5513.
- (9) Capelot, M.; Montarnal, D.; Tournilhac, F.; Leibler, L. Metal-Catalyzed Transesterification for Healing and Assembling of Thermosets. J. Am. Chem. Soc. 2012, 134, 7664–7667.
- (10) Montarnal, D.; Capelot, M.; Tournilhac, F.; Leibler, L. Silica-Like Malleable Materials from Permanent Organic Networks. *Science* **2011**, 334, 965–968.
- (11) Porath, L. E.; Evans, C. M. Importance of Broad Temperature Windows and Multiple Rheological Approaches for Probing Viscoelasticity and Entropic Elasticity in Vitrimers. *Macromolecules* **2021**, *54*, 4782–4791.
- (12) Kang, B.; Kalow, J. A. Internal and External Catalysis in Boronic Ester Networks. *ACS Macro Lett.* **2022**, *11*, 394–401.
- (13) Chen, L.; Zhang, L.; Griffin, P. J.; Rowan, S. J. Impact of Dynamic Bond Concentration on the Viscoelastic and Mechanical Properties of Dynamic Poly(Alkylurea-Co-Urethane) Networks. *Macromol. Chem. Phys.* **2020**, 221, 1900440.
- (14) Van Lijsebetten, F.; De Bruycker, K.; Winne, J. M.; Du Prez, F. E. Masked Primary Amines for a Controlled Plastic Flow of Vitrimers. *ACS Macro Lett.* **2022**, *11*, 919–924.
- (15) Azcune, I.; Odriozola, I. Aromatic Disulfide Crosslinks in Polymer Systems: Self-healing, Reprocessability, Recyclability and More. *Eur. Polym. J.* **2016**, 84, 147–160.
- (16) Canadell, J.; Goossens, H.; Klumperman, B. Self-Healing Materials Based on Disulfide Links. *Macromolecules* **2011**, 44, 2536–2541.
- (17) Lewis, B.; Dennis, J. M.; Shull, K. R. Effects of Dynamic Disulfide Bonds on Mechanical Behavior in Glassy Epoxy Thermosets. ACS Appl. Polym. Mater. 2023, 5, 2583–2595.
- (18) Rusayyis, M. A. B.; Torkelson, J. M. Reprocessable Covalent Adaptable Networks with Excellent Elevated-Temperature Creep Resistance: Facilitation by Dynamic, Dissociative Bis(hindered amino) Disulfide Bonds. *Polym. Chem.* **2021**, *12*, 2760–2771.
- (19) Jourdain, A.; Asbai, R.; Anaya, O.; Chehimi, M. M.; Drockenmuller, E.; Montarnal, D. Rheological Properties of Covalent Adaptable Networks with 1,2,3-Triazolium Cross-Links: The Missing

- Link between Vitrimers and Dissociative Networks. *Macromolecules* **2020**, *53*, 1884–1900.
- (20) Zhang, V.; Kang, B.; Accardo, J. V.; Kalow, J. A. Structure–Reactivity–Property Relationships in Covalent Adaptable Networks. *J. Am. Chem. Soc.* **2022**, *144*, 22358–22377.
- (21) Martins, M. L.; Zhao, X.; Demchuk, Z.; Luo, J.; Carden, G. P.; Toleutay, G.; Sokolov, A. P. Viscoelasticity of Polymers with Dynamic Covalent Bonds: Concepts and Misconceptions. *Macromolecules* **2023**, *56*, 8688–8696.
- (22) Zhang, L.; Chen, L.; Rowan, S. J. Trapping Dynamic Disulfide Bonds in the Hard Segments of Thermoplastic Polyurethane Elastomers. *Macromol. Chem. Phys.* **2017**, *218*, 1600320.
- (23) Lessard, J. J.; Stewart, K. A.; Sumerlin, B. S. Controlling Dynamics of Associative Networks through Primary Chain Length. *Macromolecules* **2022**, *55*, 10052–10061.
- (24) Dobbins, D. J.; Scheutz, G. M.; Sun, H.; Crouse, C. A.; Sumerlin, B. S. Glass-Transition Temperature Governs the Thermal Decrosslinking Behavior of Diels—Alder Crosslinked Polymethacrylate Networks. *J. Polym. Sci.* **2020**, *58*, 193—203.
- (25) Ediger, M. D.; Angell, C. A.; Nagel, S. R. Supercooled Liquids and Glasses. J. Phys. Chem. 1996, 100, 13200-13212.
- (26) Qin, Q.; McKenna, G. B. Correlation between Dynamic Fragility and Glass Transition Temperature for Different Classes of Glass Forming Liquids. *J. Non-Cryst. Solids* **2006**, 352, 2977–2985.
- (27) Sokolov, A. P.; Novikov, V. N.; Ding, Y. Why Many Polymers are so Fragile. J. Phys.: Condens. Matter 2007, 19, 205116.
- (28) Biedermann, F.; Schneider, H.-J. Experimental Binding Energies in Supramolecular Complexes. *Chem. Rev.* **2016**, *116*, 5216–5300.
- (29) Samanta, S.; Kim, S.; Saito, T.; Sokolov, A. P. Polymers with Dynamic Bonds: Adaptive Functional Materials for a Sustainable Future. *J. Phys. Chem. B* **2021**, *125*, 9389–9401.
- (30) Elling, B. R.; Dichtel, W. R. Reprocessable Cross-Linked Polymer Networks: Are Associative Exchange Mechanisms Desirable? *ACS Cent. Sci.* **2020**, *6*, 1488–1496.
- (31) Matxain, J. M.; Asua, J. M.; Ruipérez, F. Design of New Disulfide-Based Organic Compounds for the Improvement of Self-Healing Materials. *Phys. Chem. Chem. Phys.* **2016**, *18*, 1758–1770.
- (32) Locati, G.; Tobolsky, A. V. Studies of the Toughness of Polycarbonate of Bisphenol a in Light of its Secondary Transition. *Adv. Mol. Relax. Process.* **1970**, *1*, 375–408.
- (33) Vincent, P. I. Impact Strength and Mechanical Losses in Thermoplastics. *Polymer* **1974**, *15*, 111–116.
- (34) Chen, L. P.; Yee, A. F.; Goetz, J. M.; Schaefer, J. Molecular Structure Effects on the Secondary Relaxation and Impact Strength of a Series of Polyester Copolymer Glasses. *Macromolecules* **1998**, 31, 5371–5382
- (35) Charlesworth, J. M. Effect of Crosslink Density on the Molecular Relaxations in Diepoxide-Diamine Network Polymers. Part 1. The Glassy Region. *Polym. Eng. Sci.* 1988, 28, 221–229.
- (36) Cukierman, S.; Halary, J.-L.; Monnerie, L. Dynamic Mechanical Response of Model Epoxy Networks in the Glassy State. *Polym. Eng. Sci.* 1991, 31, 1476–1482.
- (37) Delannoy, R.; Quélennec, B.; Tognetti, V.; Delbreilh, L.; Delpouve, N.; Richaud, E. Glass and Sub-Glass Relaxation Changes Induced by Thermal Ageing of Epoxy-Amine Polymer Networks—A DMA Study. *Polym. Degrad. Stab.* **2023**, 216, 110487.
- (38) Soles, C. L.; Burns, A. B.; Ito, K.; Chan, E. P.; Douglas, J. F.; Wu, J.; Yee, A. F.; Shih, Y.-T.; Huang, L.; Dimeo, R. M.; Tyagi, M. Why Enhanced Subnanosecond Relaxations Are Important for Toughness in Polymer Glasses. *Macromolecules* **2021**, *54*, 2518–2528.
- (39) Takahashi, A.; Ohishi, T.; Goseki, R.; Otsuka, H. Degradable Epoxy Resins Prepared from Diepoxide Monomer with Dynamic Covalent Disulfide Linkage. *Polymer* **2016**, *82*, 319–326.
- (40) Memon, H.; Wei, Y. Welding and Reprocessing of Disulfide-Containing Thermoset Epoxy Resin Exhibiting Behavior Reminiscent of a Thermoplastic. *J. Appl. Polym. Sci.* **2020**, *137*, 49541.
- (41) Li, L.; Chen, X.; Jin, K.; Torkelson, J. M. Vitrimers Designed Both to Strongly Suppress Creep and to Recover Original Cross-Link

- Density after Reprocessing: Quantitative Theory and Experiments. *Macromolecules* **2018**, *51*, 5537–5546.
- (42) Kumar, R.; Goswami, M.; Sumpter, B. G.; Novikov, V. N.; Sokolov, A. P. Effects of Backbone Rigidity on the Local Structure and Dynamics in Polymer Melts and Glasses. *Phys. Chem. Chem. Phys.* **2013**, *15*, 4604–4609.
- (43) Dudowicz, J.; Freed, K. F.; Douglas, J. F. Advances in Chemical Physics. Chapter 3; John Wiley & Sons, Ltd, 2007; pp 125–222.
- (44) Mei, B.; Lin, T.-W.; Sheridan, G. S.; Evans, C. M.; Sing, C. E.; Schweizer, K. S. Structural Relaxation and Vitrification in Dense Cross-Linked Polymer Networks: Simulation, Theory, and Experiment. *Macromolecules* **2022**, *55*, 4159–4173.
- (45) Schenk, V.; De Calbiac, J.; D'Elia, R.; Olivier, P.; Labastie, K.; Destarac, M.; Guerre, M. Epoxy Vitrimer Formulation for Resin Transfer Molding: Reactivity, Process, and Material Characterization. *ACS Appl. Polym. Mater.* **2024**, *6*, 6087–6095.
- (46) Hill, A. J.; Agrawal, C. M. Positron Lifetime Spectroscopy Characterization of Thermal History Effects on Polycarbonate. *J. Mater. Sci.* **1990**, 25, 5036–5042.
- (47) Dennis, J. M.; Krishnamurthy, A.; Sirk, T. W.; Patterson, B. A.; Busch, C. E.; Lenhart, J. L.; Knorr, D. B. J. Bridging Strength and Ductility in Crosslinked Epoxy Networks. *ACS Appl. Polym. Mater.* **2023**, *5*, 5082–5091.
- (48) Hempel, E.; Hempel, G.; Hensel, A.; Schick, C.; Donth, E. Characteristic Length of Dynamic Glass Transition near Tg for a Wide Assortment of Glass-Forming Substances. *J. Phys. Chem. B* **2000**, *104*, 2460–2466.
- (49) Sasaki, T.; Uchida, T.; Sakurai, K. Effect of Crosslink on the Characteristic Length of Glass Transition of Network Polymers. *J. Polym. Sci., Part B: Polym. Phys.* **2006**, 44, 1958–1966.
- (50) Mammen, M.; Shakhnovich, E. I.; Whitesides, G. M. Using a Convenient, Quantitative Model for Torsional Entropy to Establish Qualitative Trends for Molecular Processes that Restrict Conformational Freedom. *J. Org. Chem.* 1998, 63, 3168–3175.
- (51) Shahin Thayyil, M.; Ngai, K.; Prevosto, D.; Capaccioli, S. Revealing the Rich Dynamics of Glass-Forming Systems by Modification of Composition and Change of Thermodynamic Conditions. *J. Non-Cryst. Solids* **2015**, *407*, 98–105.
- (52) McKenna, G. B.; Simon, S. L. 50th Anniversary Perspective: Challenges in the Dynamics and Kinetics of Glass-Forming Polymers. *Macromolecules* **2017**, *50*, 6333–6361.
- (53) Zheng, X.; Nie, W.; Guo, Y.; Douglas, J. F.; Xia, W. Influence of Chain Stiffness on the Segmental Dynamics and Mechanical Properties of Cross-Linked Polymers. *Macromolecules* **2023**, *56*, 7636–7650.
- (54) Xu, W.-S.; Douglas, J. F.; Sun, Z.-Y. Polymer Glass Formation: Role of Activation Free Energy, Configurational Entropy, and Collective Motion. *Macromolecules* **2021**, *54*, 3001–3033.
- (55) Mei, B.; Evans, C. M.; Schweizer, K. S. Self-Consistent Theory for Structural Relaxation, Dynamic Bond Exchange Times, and the Glass Transition in Polymeric Vitrimers. *Macromolecules* **2024**, *57*, 3242–3257.
- (56) Zheng, X.; Guo, Y.; Douglas, J. F.; Xia, W. Competing Effects of Cohesive Energy and Cross-Link Density on the Segmental Dynamics and Mechanical Properties of Cross-Linked Polymers. *Macromolecules* **2022**, *55*, 9990–10004.
- (57) Shundo, A.; Aoki, M.; Yamamoto, S.; Tanaka, K. Cross-Linking Effect on Segmental Dynamics of Well-Defined Epoxy Resins. *Macromolecules* **2021**, *54*, 5950–5956.